

Chapter-1

Introduction

to

Cuprate Superconductors

CHAPTER-I

INTRODUCTION TO CUPRATE SUPERCONDUCTORS

In this chapter, we present our review work on crystallographic features, electronic structure, theoretical modeling and existing recent work reported on dynamical conductivity of cuprate superconductors. The broad conclusion from our review are as follows: cuprate superconductors have layered structures and exhibits high anisotropy in normal state properties such as resistivity. They are type-II superconductors. They exhibits short coherence length, large penetration depth and large current density. The superconducting gap is of the order of $(3-4)k_B T_c$. Density of state near Fermi energy is small. Penetration depth shows linear temperature dependence in small temperature regime. Specific heat shows several anomalies. Microwave conductivity shows a broad peak in a temperature region below T_c . They are strongly correlated system and there is a controversy on whether or not they can be described using Fermi-liquid or marginal Fermi-liquid hypothesis. Majority of theorist believe that they can be better described using models related to Hubbard model.

1.1 Superconductivity: *A brief review*

Superconductivity has been a fluctuating subject since the discovery by Kammerlingh Onnes in 1911 and it appears to be the biggest revolution that has occurred in physical and material science. The superconducting state of a solid which offers no resistance to the passage of electricity and repel a magnet. The cuprate superconductors (CS) have shown several phenomena like the high transition temperature, weak isotope effect, extreme sensitive to oxygen

deficiency and electronic anisotropy. The cuprate superconductors possess layered structure with extremely pronounced anisotropy. The charge transport along *c*-axis is very different in nature than it is in *a-b* plane. There exists a definite pseudogap in underdoped CS above T_c . This was not only a favorite ground for scientists interested in the study of solid but also of intensive interest in engineers and technologists because of variety of applications. NMR imaging employed in medical diagnostics instead of traditional cat scan employing X-rays uses large superconducting materials. Many electronics, magnetic and microwave devices using superconducting materials have been fabricated. Although power transmission or energy storage using superconducting wires has not become a reality, there is every likelihood that there will soon be high speed levitating trains using superconducting technology. All these have been done with materials which become superconducting at liquid helium temperature. The discovery of the new copper oxide superconductors by Bednortz and Muller in 1986 opened up new and exciting possibilities. There have many ceramic oxide materials which become superconducting well above liquid nitrogen temperature. Efforts have been made to discover superconductor at room temperature. Figure 1.1 exhibits the systematic rise in T_c over the period of 80 years.

The different cuprate discussed hitherto can generally be said to consist of rock-salt type metal-oxygen (M-O) and defect perovskite layers. For example, $\text{La}_{2-x}\text{M}_x\text{CuO}_4$ (M=Ba or Ca), $\text{Bi}_2\text{CaSr}_2\text{Cu}_2\text{O}_8$ and $\text{TlCaBa}_2\text{Cu}_2\text{O}_7$ may be described as $[\text{La}_{1-x}\text{M}_x\text{O}]$ $[\text{La}_{1-y}\text{M}_y\text{Cu}_{3-\delta}]$, $[(\text{BiO})_2(\text{SrO})]$ $[\text{CaSr}(\text{CuO}_{3-x})_2]$ and $[(\text{TlO})(\text{BaO})]$ $[\text{Ca},\text{Ba}(\text{CuO}_{3-x})_2]$, respectively. The 123 cuprates have no rock-salt layers and contain only perovskite layers, in addition they have Cu-O chains. All of them have Cu-O planes essentially with a square pyramidal (or octahedral) coordination of Cu with an apical oxygen. The Cu-O band is quite covalent with an average distance of around 1.9 \AA . In addition to the two

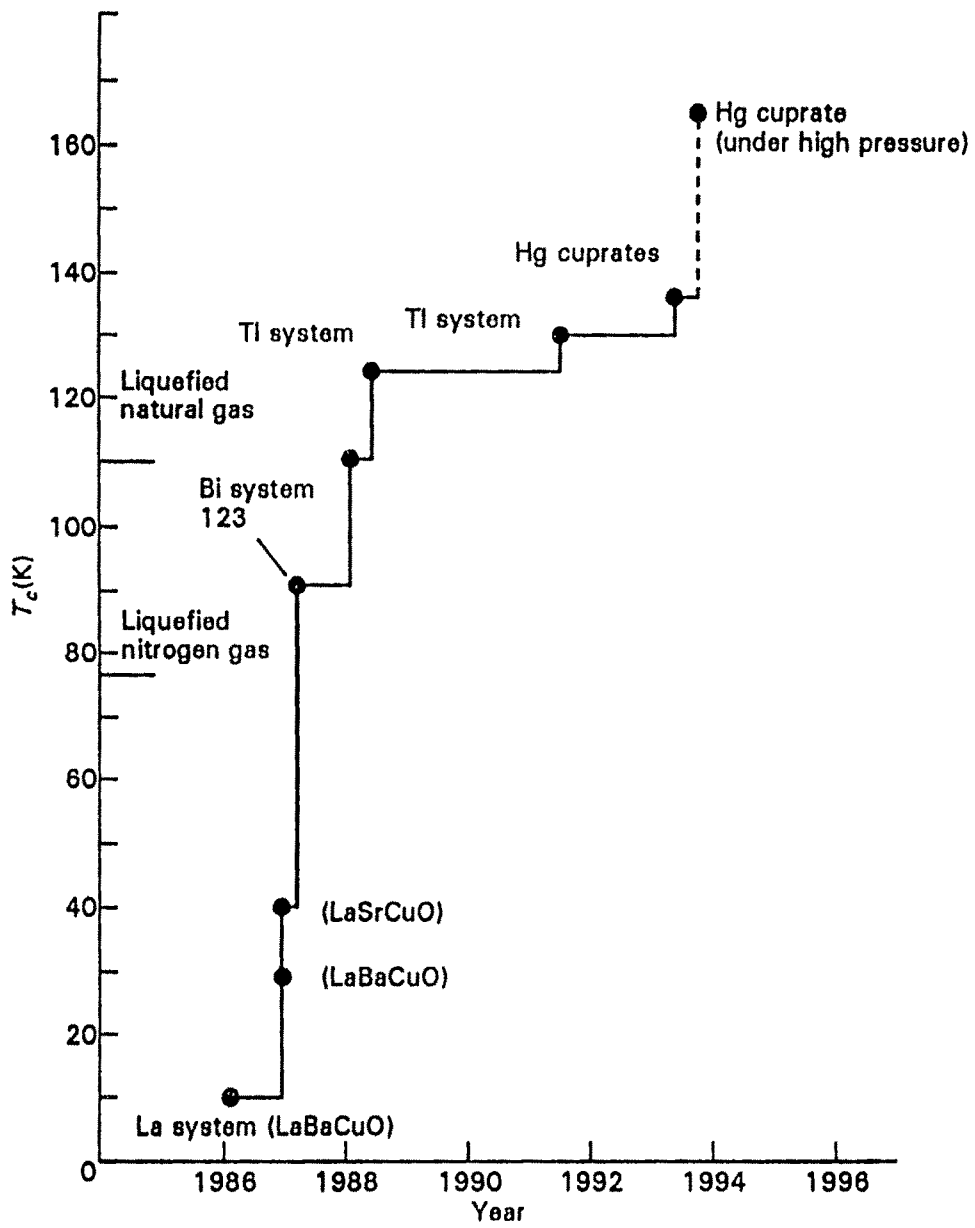


Fig. 1.1 Systematic rise in T_c .

dimensional Cu-O planes which are primarily responsible for superconductivity. They have charge reservoir in the 123 cuprates by removing the chain oxygen is not favorable for superconductivity. In Fig.1.2 the general features of the cuprates shown schematically. The superconducting cuprates generally have parent members which are antiferromagnetic insulators e.g. La_2CuO_4 , $\text{YBa}_2\text{Cu}_3\text{O}_7$ and $\text{Bi}_2\text{CaSr}_2\text{LnO}_8$.

Because of the presence of the two dimensional Cu-O planes, these materials have anisotropic properties. Accordingly, these cuprate show very much higher normal state resistivity perpendicular to the a - b plane compare to that in the plane. The mica like morphology of bismuth cuprates underscore their anisotropic nature. An important feature common to these cuprates is that they are all hole superconductors containing oxygen holes. That is the excess positive charge resides on oxygen giving rise to O^{1-} type species rather than on copper giving rise to Cu^{3+} type species. There is considerable evidence for the presence of such O^{1-} species from X-ray absorption spectroscopy and photoemission studies. In the different series of cuprates, the T_c varies with hole concentration.

Some of the important properties of the superconducting state are the anisotropy in resistivity, specific heat, critical field, critical current, magnetic penetration depth and coherence length. The resistivity of CS is found highly anisotropic . The resistivity along a - b plane is of the nature of metallic, whereas resistivity along c -axis may or may not metallic. In high temperature superconductor (HTSC) it is more than 3 order of magnitude larger than that of metallic Cu which puts HTSC with a factor of 3 or 4 of semiconductor range. The anisotropic ratio of the resistivity of different compounds is of the order of 10^2 to 10^5 at different temperature. Above T_c , the specific heat of HTSC follows the Deby's theory. Below Deby's temperature θ_D it follows the relation

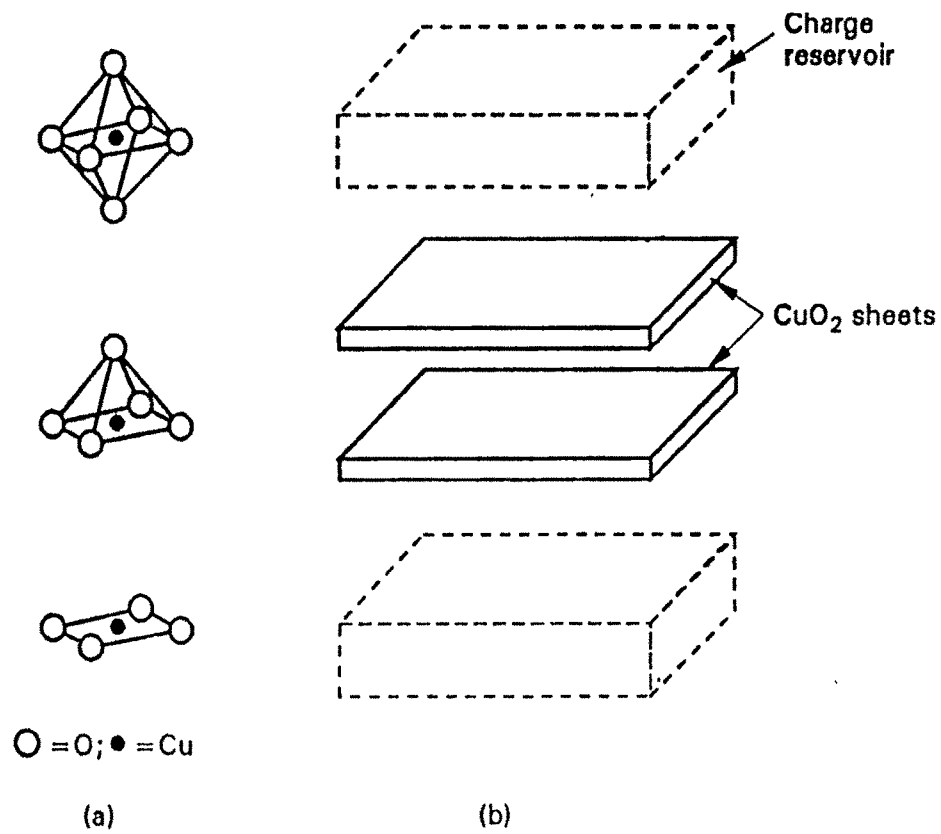


Fig. 1.2 General features of cuprates

$$C = aT^{-2} + \gamma T + AT^2, \quad (1.1)$$

where aT^{-2} is Schottky term. The BCS theory which predicts that the electronic specific heat jumps abruptly at T_c from normal state value γT_c to the superconducting state value C_s with ratio $(C_s - \gamma T_c) / \gamma T_c = 1.43$. For $T < T_c$, BCS theory predicts that the electronic contribution to the specific heat C_s will depend exponentially on temperature, $C_s = a \exp \left| -\Delta / k_B T \right|$. $\text{YBa}_2\text{Cu}_3\text{O}_7$, which by far is the most studied material among the 90 K materials, exhibits lower and upper critical fields H_{c1} and H_{c2} of 1 T and 120 T, respectively parallel to c -axis. The anisotropy in critical magnetic field is much smaller as compared to that in resistivity. Measurements on penetration depth (λ) along a - b plane and c -axis indicate that it is linear T -dependent in a particular temperature range and near T_c , $\lambda(T) \propto [1 - T/T_c]^{0.33}$. The penetration depth, $\lambda \sim 1400 \text{ \AA}$. The coherence length is generally 10 - 30 \AA in the a - b plane and around 3 \AA perpendicular to the plane. As the CS possesses a strongly interacting system of charge carriers, the carrier density (n) is of the order of 10^{21} - 10^{22} cm^{-3} , but in metallic superconductors it is of the order of 10^{23} cm^{-3} . In general, current density (J_c) along a - b plane is much larger than it is along c -axis. The experimental measurements show that near $T \approx T_c$,

$$J_c = 4J_c(0) [1 - T/T_c]^{3/2} \quad (1.2)$$

and at $T \rightarrow 0$

$$J_c = 4J_c(0) [1 - (T/T_c)^2]. \quad (1.3)$$

The critical current in both polycrystalline and single crystal materials of all the cuprates is generally small ($< 10^3 \text{ amp cm}^{-2}$) due to the presence of grain boundaries and weak flux pinning. Large current densities (10^5 - 10^6 amp cm^{-2}) have been obtained in thin films only. The superconducting gap Δ in $\text{YBa}_2\text{Cu}_3\text{O}_7$ seems to be

around $(3-4) k_B T_c$. It is found larger along a - b plane than that along c -axis. The density of the states near the Fermi energy is small in these materials.

1.2 Cuprates and their crystallographic structure

1.2.1 La_2CuO_4 cuprates

These cuprates have their ideal structure form of single rock-salt layer $[(O, Sr)O]_\infty$ intergrown pervoskite layers built up of corner sharing CuO_4 octahedra. The structure can be pictured as a stacking of CuO_4La_2 groups alternating with image La_2CuO_4 groups along c -direction as shown in Fig. 1.3 proposed by Cava et.al., Kinoshita et.al. and Longo and Raccach [1]. Another way of visualizing the structure, is by generating from the group $Cu_{1/2}O_2La$. Comprising the layer $[O - La]$ and $1/2[CuO_2 -]$ in subcell-I shown in right side of the Fig. 1.4 (the factor $1/2$ appears because the $[CuO_2 -]$ layer is shared by two subcell). Subcell-II is formed by reflection of subcell-I, and subcell-III and IV are formed from I and II. Therefore subcell I and II together contain the group CuO_4La_2 , and subcell III and IV together contain its image counterpart group La_2O_4Cu .

The layering scheme of La_2CuO_4 , consisting of equally spaced flat CuO_2 layers with their oxygen stacked one above the other, as shown in Fig. 1.5. These planes are body centred image of each other and are perfectly flat because they are reflection planes. Half of the oxygen O(I) are in the plane and the other half O(II) between the plane. The copper is octahedrally coordinated with oxygen, but the distance 1.9 \AA from Cu to O(I) in the CuO_2 planes is much less than the vertical distance of 2.4 \AA from Cu to apical oxygen O(II). The La is

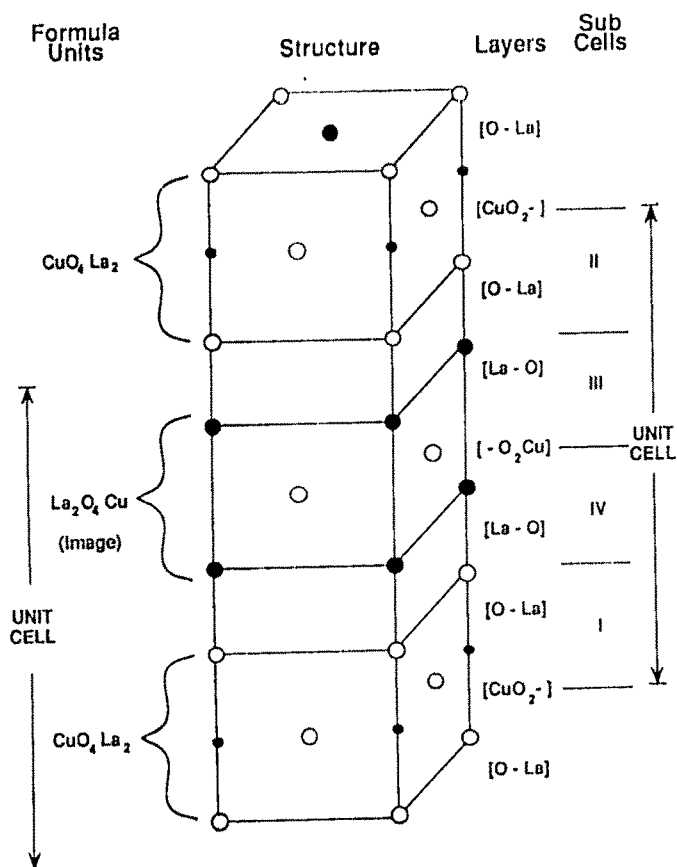


Fig. 1.3 Structure of La_2CuO_4 (centre) showing the formula units (left) and the level labels and subcell types (right). Two choice of unit cell are indicated, the left side of unit cell based on formula units and the more common right side type unit cell based on copper-oxide layers.

La_2CuO_4	Sub Cell	Nd_2CuO_4
$[\text{CuO}_2^-]$	—	$[\text{CuO}_2^-]$
$[\text{O} \cdot \text{La}]$	II	$[- \cdot \text{Nd}]$
$[\text{La} \cdot \text{O}]$	—	$[- \text{O}_2^-]$
$[\text{La} \cdot \text{O}]$	III	$[\text{Nd} \cdot \cdot]$
$[- \text{O}_2\text{Cu}]$	—	$[- \text{O}_2\text{Cu}]$
$[\text{La} \cdot \text{O}]$	IV	$[\text{Nd} \cdot \cdot]$
$[\text{O} \cdot \text{La}]$	—	$[- \text{O}_2^-]$
$[\text{CuO}_2^-]$	I	$[- \cdot \text{Nd}]$
$[\text{CuO}_2^-]$	—	$[\text{CuO}_2^-]$

Fig. 1.4 Layering scheme of La_2CuO_4 (T, left) and Nb_2CuO_4 (T, right) structures. The locations of the four subcells of the unit cell are indicated in the centre column.

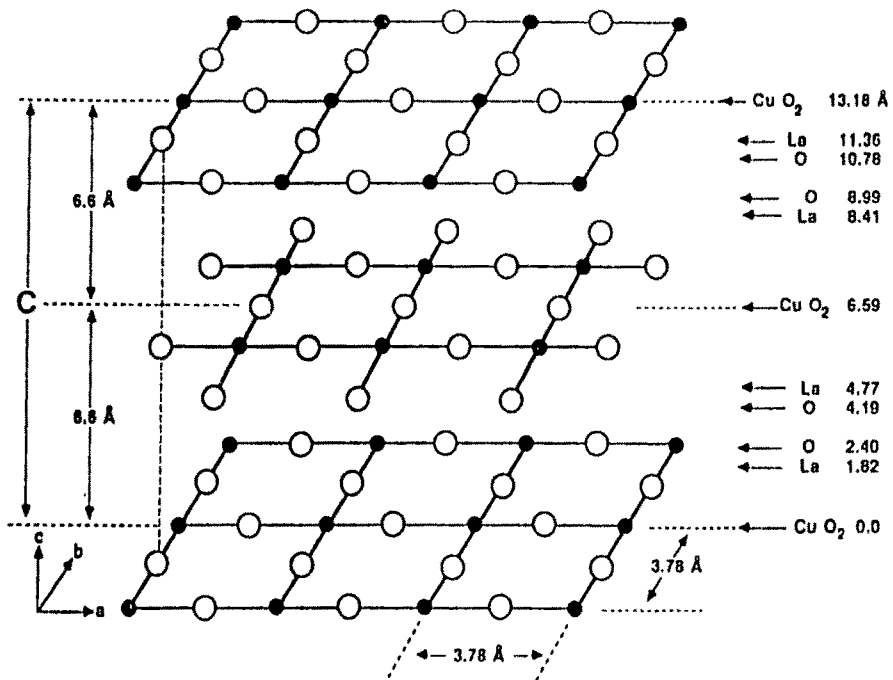


Fig. 1.5 CuO_2 layers of the La_2CuO_4 structure showing horizontal displacement of Cu atoms in alternate layer. The layers are perpendicular to the c-axis.

nine-fold coordinated to four O(I) oxygen, to four O(II) at $(1/2, 1/2, z)$ sites, and to one O(II) at a $(0, 0, z)$ site.

1.2.2 The $YBa_2Cu_3O_{7-\delta}$ cuprates

$YBa_2Cu_3O_{7-\delta}$ consists of layers of corner sharing CuO_2 pyramids linked through rows of corner sharing CuO_2 square planar groups, forming triple copper layers interleaved with yttrium planes as shown in Fig.1.6a. $YBa_2Cu_3O_6$ is derived from $YBa_2Cu_3O_{7-\delta}$ by removing the oxygen atoms of the CuO_4 groups located at the same level as copper so that pyramidal layers are linked through CuO_2 sticks as shown in Fig. 1.6b. It is worth pointing out that $YBa_2Cu_2^{II,III}O_7$ with certainly a complete delocalization of the holes over the copper-oxygen frame-work, whereas in $YBa_2Cu_3O_6$ one observed a mixed valency Cu(II)-Cu(III) which corresponds in fact to a localization of the two sorts of cations, with divalent copper in pyramidal configuration and univalent copper in two fold coordination according to the formulation $YBa_2Cu_2^{II}Cu^I O_6$.

The deviation from “ O_7 ” stoichiometry leading to the general composition $YBa_2Cu_3O_{7-\delta}$ strongly affects the superconducting properties of this material. From the work done by several groups [2-5], it has been shown that T_c decreases as δ increases from 0 to 1. The evolution of T_c was found different by different authors because of the fact that the arrangement of oxygen vacancies in the structure, depend upon the experimental methods of synthesis. X-ray diffraction and neutron diffraction studies can bring information about the structure of these phases but can only give an average structure owing to the fact that oxygen atom can be distributed in the form of microdomains even in single crystal. This is for instance the case of the tetragonal non-superconducting phase. $YBa_2Cu_3O_{6.2}$ obtain by quenching the superconductor $YBa_2Cu_3O_7$ from

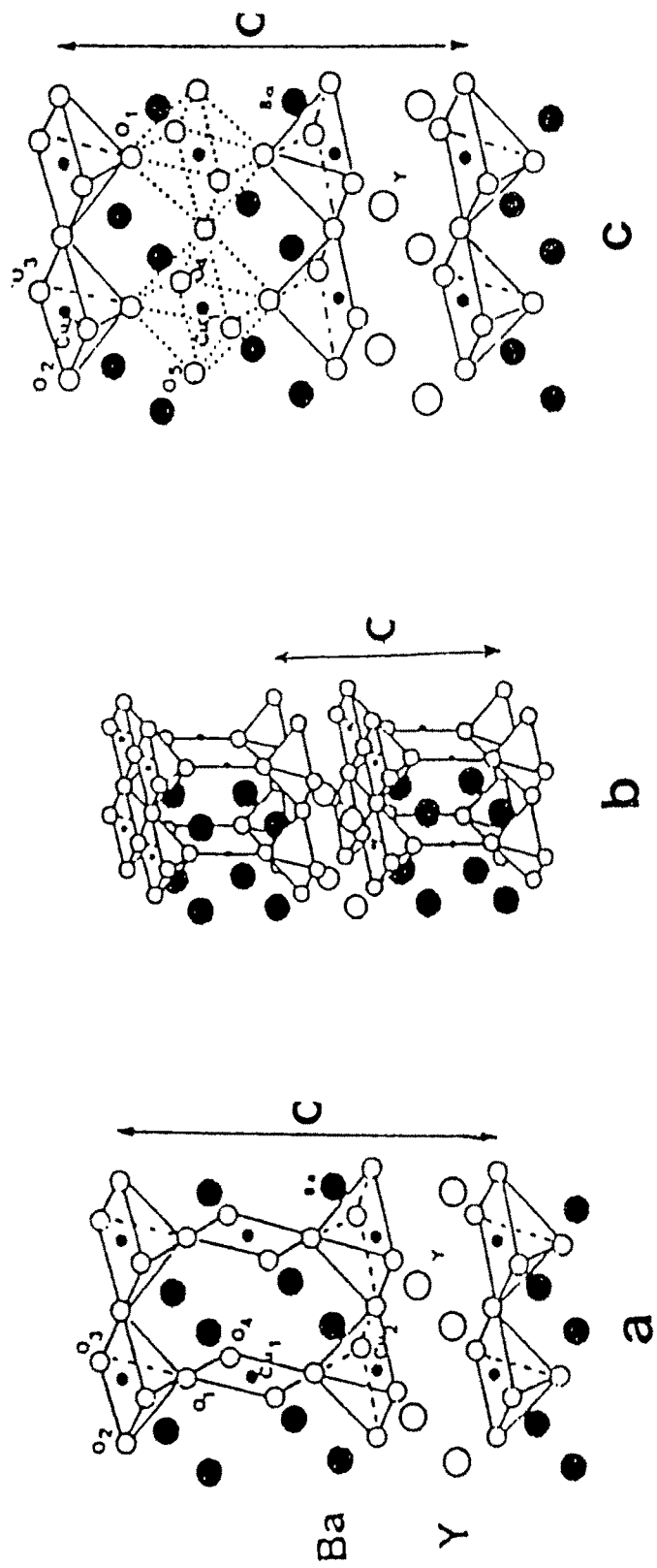


Fig.1.6 Crystal structure of YBa₂Cu₃O₇ (a), YBa₂Cu₃O₆ (b), YBa₂Cu₃O_{6.2} (c)

900^oc to room temperature. It is general agreement from X-ray diffraction on a statistical distribution of oxygen and vacancies in the basal plane of the intermediate CuO₆ octahedra located between the pyramidal layers as shown in Fig. 1.6c. The HTSC compounds have horizontal reflection plane perpendicular to the z-axis at the centre of the unit cell and another reflection plane at the top and bottom. This means that every plane of atoms in the lower half of the cell at the height z is duplicated in the upper half at the height 1-z. Such atoms appears twice in a unit cell, while atoms right on the symmetry planes only occurs once since they cannot be reflected. The Fig. 1.7 shows a [CuO₂ --] plane at a height z reflected to the height 1-z. Superconductors that have the reflection planes but lack end-centring and body-centring operation are called aligned because all of their copper atoms are of one type, either all on the edge position or all centred on c-site. In other words they all lie one above the other on the same vertical lines. The compound YBa₂Cu₃O_{7-δ} some time called YBaCuO or 123 compound in a orthorhombic form is a superconductor below transition temperature T_c= 92 K. The Fig. 1.7 above shows the localization of atoms whereas Fig. 1.8 shows arrangement of copper oxide planes. Fig. 1.9 shows that three planes containing Cu and O are sandwiched between two planes of Ba and O and one plane containing Y. The layering scheme is given on the right side of Fig. 1.7, where the superscript b on O indicates that the oxygen lies along the b-axis. The atoms are puckered in the two [Cu O₂ --] planes that have the [-- -- Y] plane between them. The third copper oxide plane [Cu O^b --] often referred to as the chains consisting the Cu-O-Cu-O chain along the b-axis in lines that are perfectly straight because they are horizontal reflection plane, where no puckering can occur. Both the copper oxide planes and chains contribute to the superconducting properties. The YBa₂Cu₃O_{7-δ} compounds comes in tetragonal and orthorhombic varieties. In the tetragonal phase the oxygen sites in the chain layer of about half occupied in a random or disordered manner and in the orthorhombic phase are ordered into -Cu-O- chains along b-direction. The

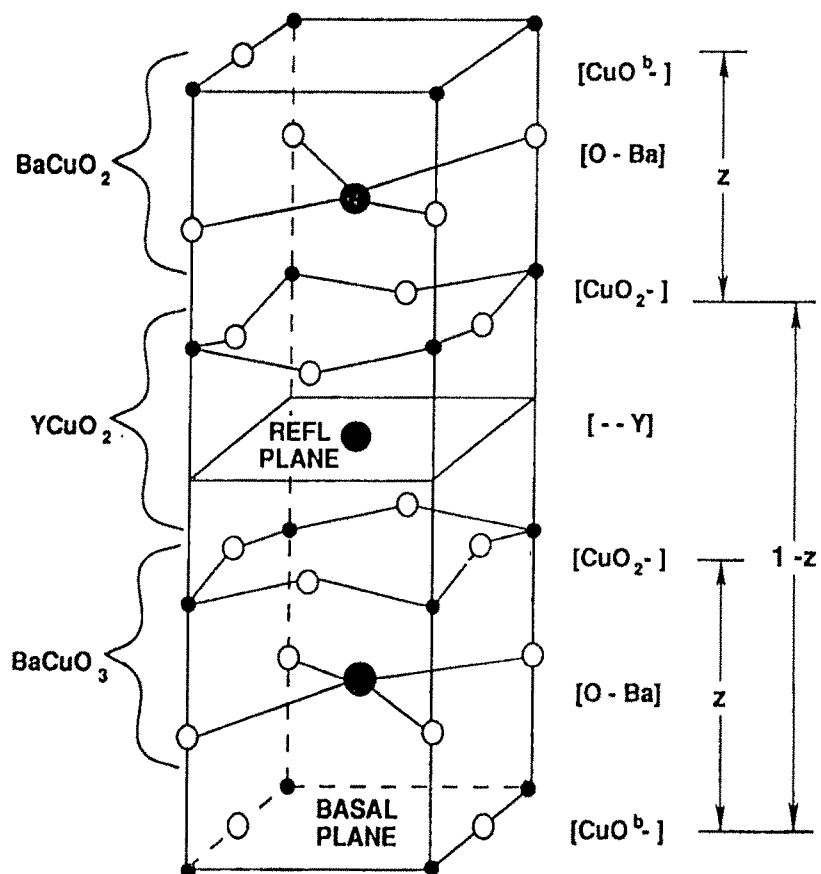


Fig. 1.7 Unit cell of $\text{YBa}_2\text{Cu}_3\text{O}_7$ showing the molecular groupings, reflection planes and layer types.

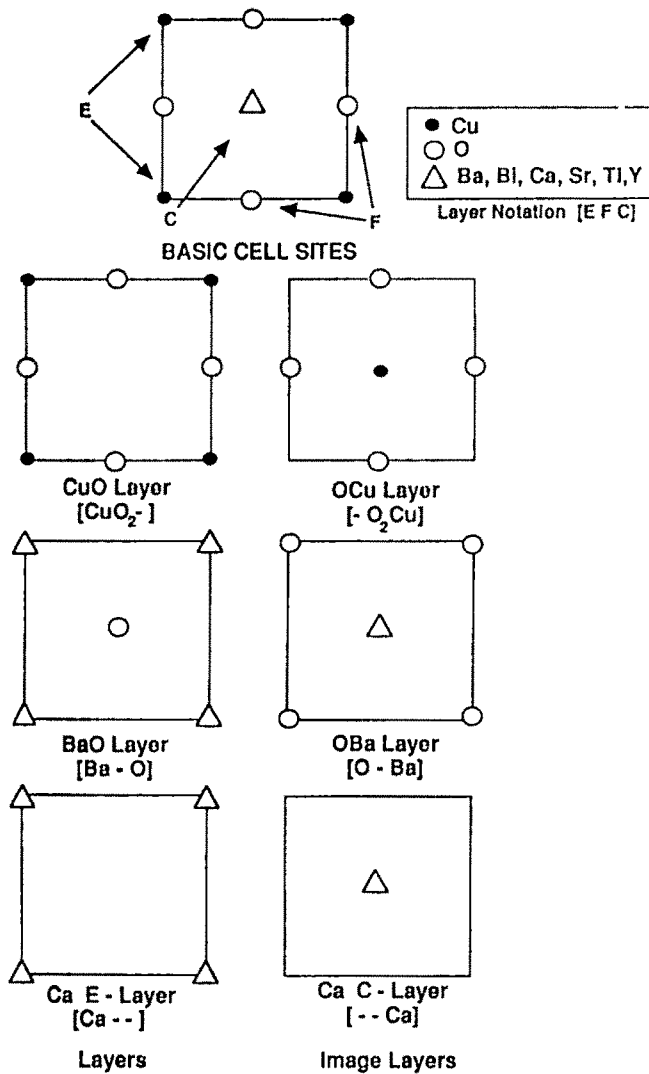


Fig.1.8 Types of atom positions in the layers of a high- T_c superconductor structure, using the edge, face and centre notation (E, F, C). Typical site occupancies are given in the upper right.

oxygen vacancy along the a -direction causes the unit cell to compress slightly so that $a < b$ and the resulting direction is of the rectangular type increasing the oxygen content so that $\delta < 0$ causes oxygen to be occupying vacant sites.

1.2.3 $\text{Bi}_2\text{Sr}_2\text{Ca}_2\text{Cu}_{n+1}\text{O}_{6+2n}$ and $\text{Tl}_2\text{Ba}_2\text{Ca}_n\text{Cu}_{n+1}\text{O}_{6+2n}$ cuprates

The compound has about same a and b lattice constants as the yttrium and lanthanum compounds, but with much larger unit cell dimension along c -axis. The series of compounds is given by general formula



where $n=0,1,2$, have essentially the same structure and same layering arrangements proposed by Barry et.al. and Siegrist et. al. [6,7], although there are some differences in detail atom positions. There are grouping of CuO_2 layers each separated from next by Ca layers with no oxygen. The CuO_2 grouping bound together by intervening layers of BiO and SrO for the bismuth compounds and intervening layers of TlO and BaO for thallium compounds. Figure 1.10 compares the layering scheme of the $\text{Tl}_2\text{Ba}_2\text{Ca}_n\text{Cu}_{n+1}\text{O}_{6+2n}$ compounds with $n=0,1,2$ with those of the lanthanum and yttrium compound. From the figure, it is also seen that the grouping of $[\text{Cu O}_2 \text{--}]$ layers and $[\text{-- O}_2 \text{Cu}]$ image planes are repeated along c -axis. A close examine of figure shows that the general stacking rules are satisfied, namely metal-ion (M-O) in adjacent layers alternate between edge (E) and centred (C) sites and adjacent layers never have oxygen on the same types of sites. The horizontal reflection symmetry of the central point of the cell is evident. Fig. 1.11 proposed by Toradi et. al. [8] presents a more graphical representation by showing position of atoms in their layers.

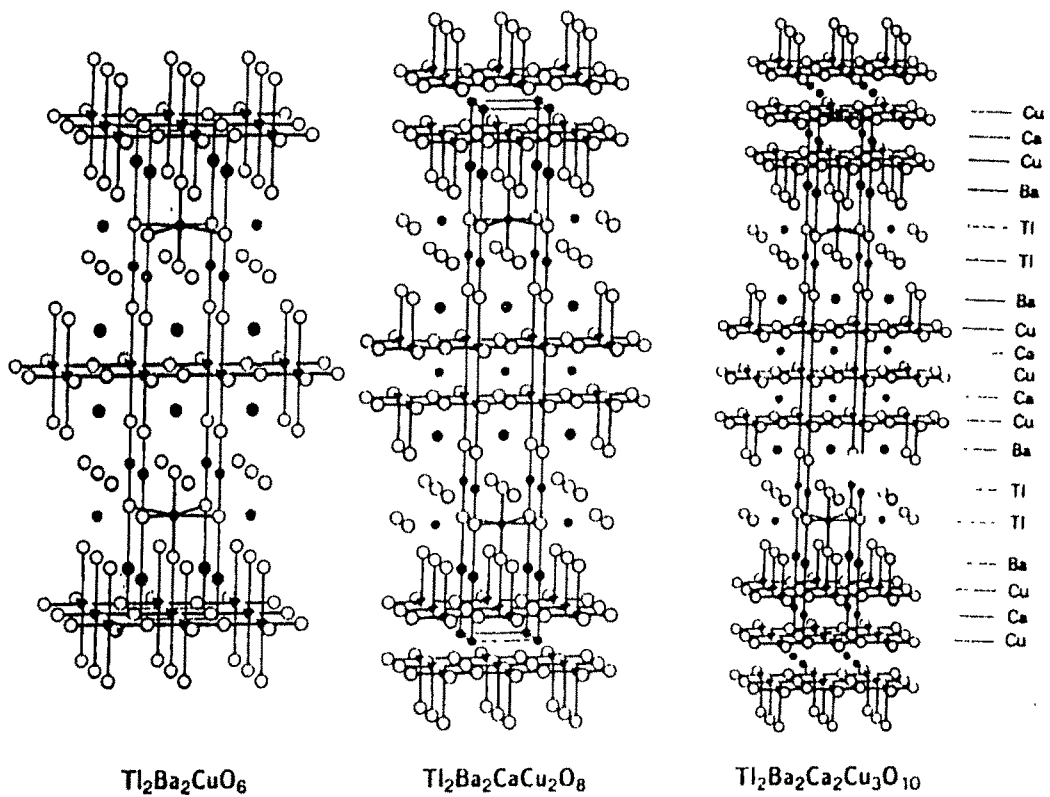


Fig. 1.11 Crystal structure of $\text{Tl}_2\text{Ba}_2\text{Ca}_n\text{Cu}_{n+1}\text{O}_{6+2n}$. superconducting compounds with $n=0,1,2$ arranged to display the layering scheme. The $\text{Bi}_2\text{Sr}_2\text{Ca}_n\text{Cu}_{n+1}\text{O}_{6+2n}$ have the same respective structure.

The thallium based compounds have higher transition temperature than their bismuth compounds [9,10]. The first member of the series namely $\text{Tl}_2\text{Ba}_2\text{CuO}_6$ with $n=0$ has no [-- -- Ca] layer and a relatively low transition about 85 K. The second member ($n=1$), $\text{Tl}_2\text{Ba}_2\text{CaCu}_2\text{O}_8$ called the 2212 compound with $T_c = 110$ K has same layering scheme as in Bi compounds. The [Cu O₂ --] layers are thicker and closer together than the corresponding layers of the bismuth compounds [11]. The third member of the series $\text{Tl}_2\text{Ba}_2\text{Ca}_2\text{Cu}_3\text{O}_{10}$ called 2223 compound has three [Cu O₂ --] layers separated from each other by [-- -- Ca] planes and has the highest transition temperature 125 K of this series of thallium compounds. It has same copper coordinates as the Bi-Sr compounds. The 2212 and 2223 compounds are tetragonal and belong to the same crystallographic space group as La_2CuO_4 .

1.2.4 *HgBa₂Ca_nCu_{n+1}O_{2n+4} cuprates*

The series of compounds



where n is integer, are prototype for the Hg family of superconductors. The first three members of the family with $n=0,1,2$ are often referred to as Hg-1201, Hg-1212 and Hg-1223, respectively. Their structure is sketched in Fig. 1.12, which was proposed by Tokiwa-Yamamoto et. al. [12]. The lattice constants are $a=3.86 \text{ \AA}$ for all of them and $c = 9.5, 12.6$ and 15.7 \AA for $n=0,1,2$, respectively. It represents the structure model for $\text{HgBa}_2\text{Ca}_n\text{Cu}_{n+1}\text{O}_{2n+4}$ for $n=0,1,2$ with mercury (Hg) located in the middle layer of the unit cell and Fig. 1.13 presents the unit cell for $n=1$ with Ca in middle [13]. It can be observed from the Fig. 1.12 that the copper atoms of Hg-1201 is in the centre of a stretched octahedron with the planer oxygen O(I) at a distance 1.96 \AA and the apical

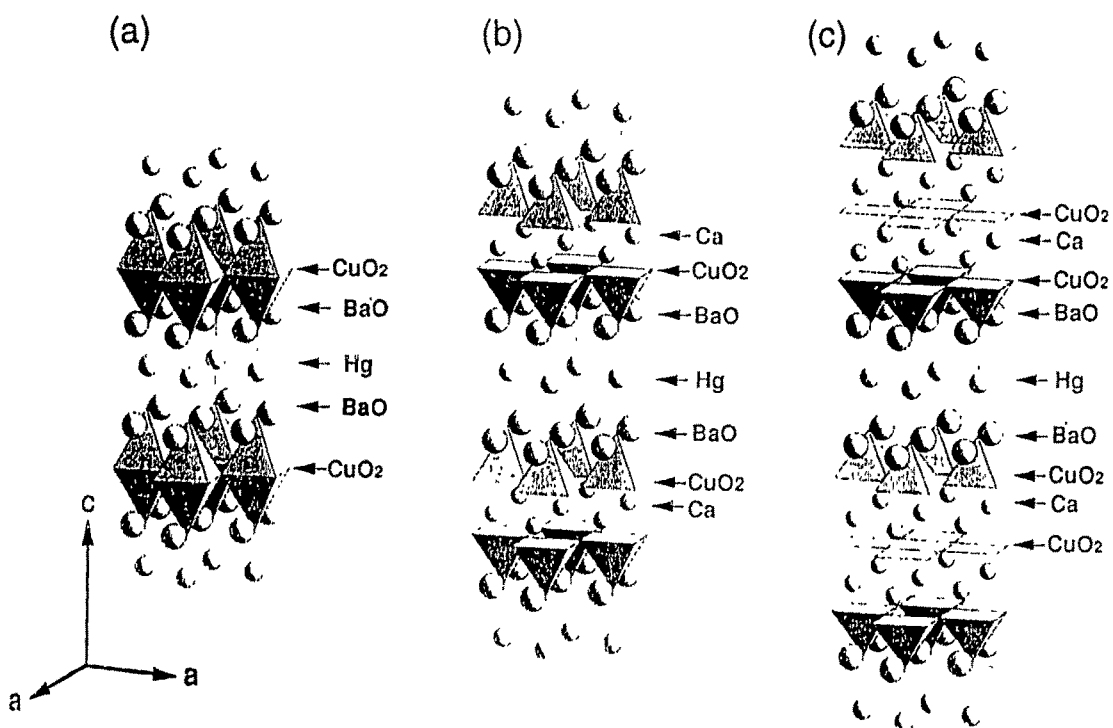


Fig. 1.12 Structure model of the series $\text{HgBa}_2\text{Ca}_n\text{Cu}_{n+1}\text{O}_{2n+4}$. The first three members with $n=0,1,2$ are shown as a, b c, respectively.

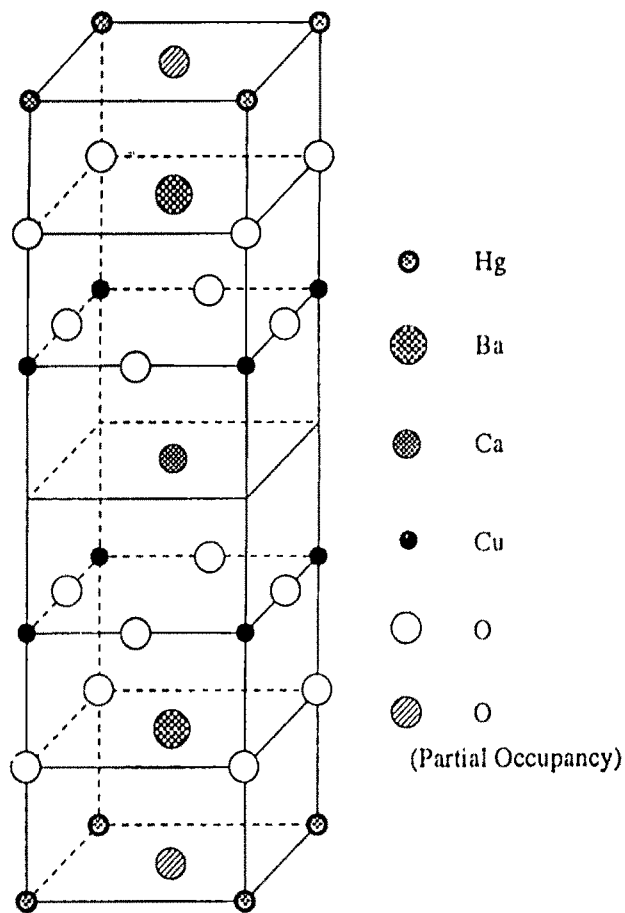


Fig. 1.13 Schematic structure of the $\text{HgBa}_2\text{Ca}_n\text{Cu}_{n+1}\text{O}_{2n+4}$ compounds.

oxygen O(II) of the [O - Ba] layer much farther away (2.78 \AA). For $n=1$, each copper atom is in the centre of the base of tetragonal pyramid and for $n=2$ the additional CuO_2 layer has Cu atoms which are square planer coordinated. As per layering scheme, Hg series have metal ions in adjacent layers alternating between edge and centred site and oxygen in adjacent layers always at different site.

1.3 Electronic structure of cuprates

An understanding of the basic electronic structure in the high- T_c cuprates has been developed based on various observations of the superconducting compositional regions as well as of the adjacent semiconducting and metallic regions [14,15]. This review mainly emphasizes that high- T_c superconductivity manifests itself in the vicinity of the semiconductor to the metal transition, which is suggested by high-level carrier doping in a superconductor with a non-conventional energy gap at the half filled position. The change in the electronic structure is symmetrical on doping in the hole and electron superconductors. In order to clarify the mechanism of the recently discovered high- T_c superconductivity in the cuprates [16,17], it is essential to understand their unique electronic structure in the normal state because the superconductivity is obtained when the electronic structure is slightly modify through weak interactions on the energy scale $k_B T_c$. The normal state electronic structure determine by stronger interactions, is essentially presented in the superconducting state. A remarkable structure features commonly encountered in the cuprate superconductors is the presence of the two dimensional network of Cu-O bands or CuO_2 square lattice. Because the typical ionic bond length of Cu-O is 0.21 nm , the significantly shortened Cu-O inter-atomic spacing about 0.19 nm , indicates the enhanced contributions from covalent bonding. Due to the square plane symmetry around the Cu-O atoms, the degeneracy of 3d orbitals is

filled as shown in Fig. 1.14. Therefore more likely covalent bond is obtained from the filling of electrons in the bonding orbitals of $\text{Cu}_{3d(x^2-y^2)}\text{O}_{2p}$ and half filling of the antibonding orbital, σ_{dp}^* . A conceptual σ_{dp}^* network expected to give the conduction band is illustrated in Fig. 1.15.

Since the Cu-O spacing along the c -axis is as large as 0.22 nm, covalent bonding along this direction should be insignificant. The electrical conduction in these cuprates therefore is expected to be essentially two-dimensional, which might be modeled by assuming pile of alternating ultra thin metallic and insulating layers. Whether the electron transfer in the c -axis is metallic or semiconductor has been a matter of controversy [18]. But recent results on a large high quality single crystal of $\text{La}_2\text{Sr}_2\text{CuO}_4$ several millimeter along c -axis below tetragonal to orthorhombic phase transition temperature and is metallic above transition. Therefore the transition probability from a metallic plane to the adjacent one across the intervening insulating ionic layer seems to be a sensitive function of the nature of the ionic layer. Important superconducting parameter such as coherence length- ξ along the c -axis are dependent upon interlayer coupling. The upper limit of the critical current could be estimated from the normal state resistivity along the c -axis by assuming Josephson coupling between the 2D metallic layers [19]. The sharp dependence of the composition on T_c was already a subject of interest well before the discovery of high- T_c superconductors in cuprates [20], one is led to assume that an energy gap opens as the half-filled position in the conduction band for some reason. The cuprate superconductors are obtained by doping the divalent Cu compounds e.g. La_2CuO_4 , which was found semiconductor because of the opening of an energy gap in the half-filled position in the conduction band due to strong electronic conduction.

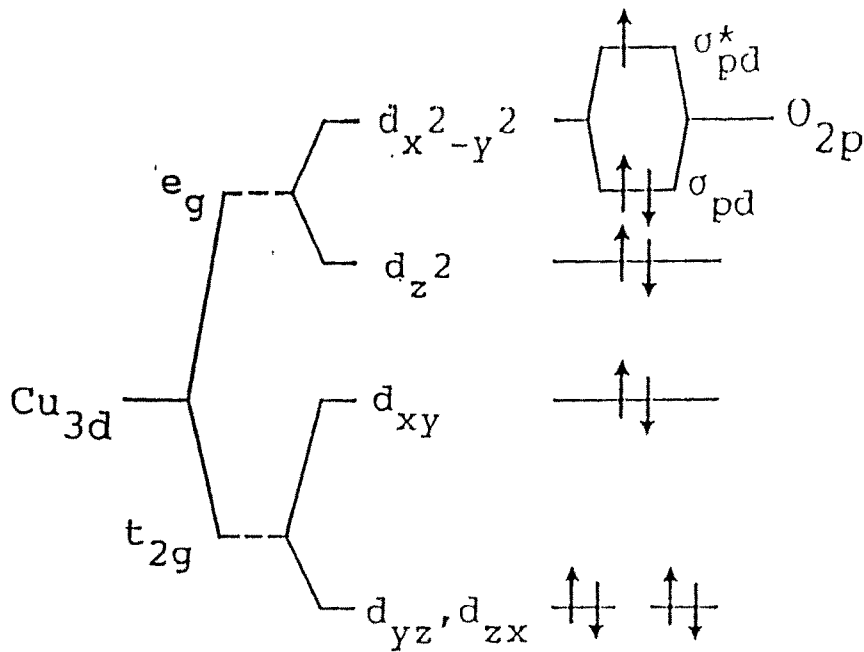


Fig. 1.14 Splitting of 3d orbital energy in the square coordinated environment. Since Cu(II) has nine 3d electrons, a hole is created at the $d(x^2-y^2)$ level. This forms a σ bond with the oxygen 2p orbital extended toward the Cu atoms, leaving a hole in the anti-bonding σ^* (dp) orbital.

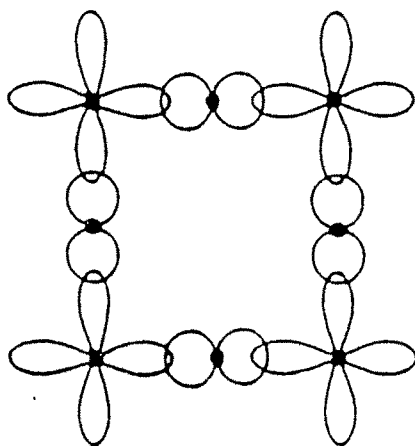


Fig. 1.15 A schematic network of σ^* (dp) bonds in the basal CuO_2 plane.

1.4 Theoretical modeling of cuprate superconductors

Present theories can be divided into two categories: (i) BCS type and (ii) non-BCS type. BCS type theories believe that there exist strongly interacting carrier gas which has Fermi-liquid behavior and pairs are formed below T_c via exchange of phonons, plasmons, excitons, spinons etc. Theoretical calculations based on resonant valence bond and t-J coupling model come under non-BCS type theories. Transport properties of cuprates such as resistivity and Hall-effect are often described using Fermi-liquid hypothesis. Anomalies of normal state properties ascribed to marginal Fermi-liquid theory. Anderson attributed the superconductivity of cuprates to break down of Fermi-liquid theory and suggested the applicability of what are called Luttinger liquids. Hubbard model, t-J model have also been applied to Fermi-liquid. Optimally doped cuprate superconductors possess Fermi surface and they are essentially metallic. Band structure calculations seem to predict shape of Fermi surface with considerable accuracy. A brief description of various models (hypothesis) is given below.

1.4.1 Fermi-liquid hypothesis

When the electrons constitute to obey Fermi-Dirac statistics and interact each other in such a manner that their properties remain close to those of a Fermi gas may be called Fermi-liquid. London (1957) developed a method of electron-electron interaction in such a manner as to maintain a one-to-one correspondence between the states of free electron gas and those of the interacting electron system. The existence of such a one-to-one correspondence constitutes the usual definition of Fermi-liquid. According to Fermi-liquid hypothesis, the Pauli's exclusion principle permits electrons to experience only momentum changing collision at Fermi surface. Elementary excitations of quasiparticle and quasiholes correspond to those of Fermi gas. In what are

called marginal Fermi-liquids, the one-to-one correspondence condition breaks down at the Fermi surface but many of the properties continue to resemble those of a Fermi-liquid. The Fermi-liquid theory has been applied to cuprate superconductors. It gives reasonably good description of normal state superconductor. System of interacting particles (electrons) can be discussed by a generalized BCS Hamiltonian given below

$$H_{\text{BCS}} = \frac{1}{2} \sum_{\mu, \mathbf{k}} \lambda_{\mu}(\mathbf{k}) \times [a_{\mu}^{\dagger}(\mathbf{k}) a_{\mu}(\mathbf{k}) - a_{\mu}^{\dagger}(\mathbf{k}) a_{\mu}(\mathbf{k})], \quad (1.6)$$

where $\lambda_{\mu}(\mathbf{k})$ is single quasiparticle energy eigen value of state μ . $a_{\mu}^{\dagger}(\mathbf{k})$ and $a_{\mu}(\mathbf{k})$ are creation and annihilation operator, respectively.

1.4.2 Hubbard model

There is a broad agreement on the microscopic Hamiltonian which can describe the electronic degrees of freedom in the energy and parameter range of interest. Also it is a variant of a lattice based interacting electron model, the family is known as a Hubbard model. Many of the most interesting properties of the material such as magnetic ordering and superconductivity require theories that go beyond independent electron approximation. In order to understand phenomena, it is necessary to take into account electron correlations. The simplest model of correlated electrons is the one state Hubbard model. Since the model is expressed in terms of a basic function called Wannier function. The Wannier function incorporates tight-binding approximation. A summation of Bloch states (which are superposition of atomic function over lattice position) provides a new wave-function known as Wannier state. In a one-state Hubbard model, there is one electron orbital per unit cell. The Hamiltonian consists of kinetic energy term proportional to hopping amplitude(t), electron correlation

contributing terms of chemical potential(μ) and on-site Coulomb repulsion(U). It has been assumed that the chemical potential explain the properties of modes as number of electron varied, whereas coulomb repulsion is same for all sites. A simpler one-band Hubbard model is based on the realization that a p-hole and neighbouring d-hole tend to form a spin singlet. This is most stable when the p-holes states around a given d-site are mixed such that the mixture has local $d_{x^2-y^2}$ symmetry. This singlet can be thought of as a spinless hole in the d-site for each added p-hole, which then eliminated from the picture. One thus work only with d-sites and the Hamiltonian

$$H = \sum_{i\sigma} \epsilon_d a_{d i \sigma}^\dagger a_{d i \sigma} + \sum_{ij\sigma} t_{ij} a_{d i \sigma}^\dagger a_{d j \sigma} + U \sum_i n_{d i \uparrow} n_{d i \downarrow} \quad (1.7)$$

where t_{ij} is effective amplitude for the d-hole to hop from site i to j . Usually, nearest neighbour hops have the largest amplitude. The average number of spinless d-holes per site is x , where x is doping. For purposes of working with the Hamiltonian, it is simpler to think of a collection with one d-electron (on the average) per site, each with spin 1/2 and of removing a fraction x of such site.

1.4.3 *t-J model*

In variant of the Hubbard model called the t-J model, the coulomb term U in the Hubbard model is replaced by Heisenberg term $J \sum S_i S_j$. This model may be obtain as the large- U limit ($U \gg t$) of the Hubbard model [21]. The effective Hamiltonian for the subject of states can written in Heisenberg form

$$H_{\text{heis}} = -J \sum S(k) S(k') \quad (1.8)$$

where the exchange coupling is

$$J = 4t^2/U. \quad (1.9)$$

Typical values of the parameters gives the value of J around 0.14 - 0.16 eV. It has been conclude that at half-filling in the limit $U/t \rightarrow \infty$, the ground state of the Hubbard model is equivalent to that of Heisenberg antiferromagnet [22]. The Heisenberg term used in the t-J model corresponds to the Hamiltonian

$$H = -t \sum (a_{i\sigma}^\dagger a_{j\sigma} + a_{j\sigma}^\dagger a_{i\sigma}) + J \sum S_i S_j \quad (1.10)$$

Underdoped material can be understood in terms of the two-dimensional Heisenberg term and in the presence of empty site the hopping matrix element t can represent hole propagation in a fluctuation antiferromagnet background arising from this $J \sum S_i S_j$ term. Many believe that t-J model embraces the essential features of high- T_c superconductivity. The symbole t-J is used to designate two terms in the Hamiltonian.

1.4.4 Resonant Valence Bond model (RVB)

While some exact results for the ground state are known in the limit $U/t \rightarrow \infty$ and for the case of half-filling, the the nature of the ground state for arbitrary U and t are not known, for ilucidation the nature of the low-lying levels of the model makes use of “Resonant Valence Bond” (RVB) states [23]. Electrons at nearest neighbour sites are paired into ‘bands’ and linear contribution of the basic states are used to construct eigenstates of the total electronic spin. For two electrons the total spin s can be 1 or 0 and the corresponding triplet ($s=1, M=0, \pm 1/2$) and singlet ($s=M=0$) wave functions are, respectively,

$$\begin{aligned} |1\ 1\rangle &= |+\ +\rangle \\ |1\ 0\rangle &= 1/\sqrt{2} (|+\ -\rangle + |-\ +\rangle) \quad \text{triplet, } E=0 \end{aligned} \quad (1.11)$$

$$|1-1\rangle = |- -\rangle$$

$$|VB\rangle = 1/\sqrt{2} (|+ -\rangle - |- +\rangle) \quad \text{singlet, } E=-4t^2/U \quad (1.12)$$

There are two additional ionised states $|A\rangle$ and $|B\rangle$

$$|A\rangle = 1/\sqrt{2} (|0 \pm\rangle - |\pm 0\rangle), \quad E=U \quad (1.13)$$

$$|B\rangle = 1/\sqrt{2} (|0 \pm\rangle + |\pm 0\rangle), \quad E=U+4t^2/U \quad (1.14)$$

and the states in which there are no electrons

$$|Vaccum\rangle = |0 0\rangle. \quad (1.15)$$

The singlet states with the electron label $|VB\rangle$ and has lowest energy constitutes “valence -band” state. The RVB theory starts by assuming the ground state of insulating La_2CuO_4 is a linear contribution of $|VB_{ij}\rangle$ states for various pairs of electrons i, j .

$$|RVB\rangle = c_{12}|VB12\rangle + c_{34}|VB34\rangle + c_{56}|VB56\rangle + \dots \quad (1.16)$$

and in a presence of single hole with spin down ($h -$) paired with a spin up electron ($e +$), this becomes

$$|RVB, 1 \text{ hole}\rangle = c_{12}|h -\rangle |e +\rangle + c_{34}|VB34\rangle + c_{56}|VB56\rangle + \dots \quad (1.17)$$

where the hole can between sites. The RVB approach has been used to explain high- T_c superconductivity but has not found wide application.

1.5 Dynamical conductivity of cuprate superconductors: A review on existing work

In recent years numerous careful experiments have been made on the cuprate superconductors and with involvement on sample quality, many of the strange phenomena observed in these materials. In particular, there is strong evidence for an unconventional pairing state predominantly of $d_{x^2-y^2}$ symmetry [24]. Surface impedance ($Z_s=R_s+iX_s$) measurements probe the complex conductivity ($\sigma=\sigma_1-i\sigma_2$) of a superconductor as a function of frequency (ω) and temperature (T). In the case of local electrodynamics, which applies to the cuprates, the relationship between Z_s and σ is $Z_s=\{i\mu_0\omega/\sigma\}^{1/2}$. At low frequencies and at temperature not close to T_c , one can accurately make the approximation $R_s=1/2\{\mu_0^2\lambda^3\omega^2\sigma_1\}$ and $X_s=\mu_0\lambda\omega$. It is usual to interpret the complex conductivity in terms of two-fluid model and various authors [25] discussed the validity of partitioning the conduction electron density in to normal and superfluid fraction n_n and n_s ($n_n+n_s=1$) and conclude that this is appropriate in London limit. There have been a large number of investigations on frequency ω and temperature T dependent dynamical conductivity of normal as well as superconducting state of HTSC during recent past years. It is not possible to review all papers which have been published dynamical conductivity of HTSC. A review based on some of the papers reporting salient feature on dynamical conductivity is presented in this section.

1.5.1 Frequency dependent dynamical conductivity

Infra-red conductivity has been widely used to get information about the properties of superconducting state. As a probe of particle-hole excitation spectrum of superconductor, infra-red conductivity contain interaction on the value of the energy gap as well as on the coupling of electrons to the low-lying

excitations in which they are coupled. For example, the phonon in the case of conventional superconductors and perhaps as yet unidentified because in the case of high- T_c oxides. In dirty limit (mean free path $l < \xi$) and for a BCS superconductor, the well known expression of Mattis and Bardeen for the ω -dependence of real part of the conductivity, $\sigma_1(\omega)$ applies and there is no absorption until $\omega=2\Delta$, (i.e. until twice the value of energy gap) is reached at which point the absorption increases sharply from zero towards its normal state value. The sharp absorption gives the measure of the gap. Infra-red studies of the classical low temperature superconductors provided the existence of the superconducting energy gap as well as information on the plasma mediated pairing interactions [26,27]. At particular T/T_c , the conductivity of a superconductor when $\omega>2\Delta$ shows a onset [28]. The a - b plane conductivity which avoids chain is believed to provide a probe of the properties of CuO_2 planes. It has been proposed [29] that the behaviour of the conductivity in normal state reflects a two component response consisting “free carriers” Drude piece and a midinfra-red contributions associated with “bound carriers”. Likewise, in the superconducting state, various explanations of the data regarding component picture [29-31] argued that the “free carriers” condensed to form a superfluid, while the “bound carriers” giving rise in the midinfra-red structure which becomes more clearly visible below T_c . There have been several explanation for the structure for the infra-red data based on a gap with modes.

Theoretical investigations on how anisotropy in the pairing interaction gets reflected in the ac optical conductivity of the Eliashberg superconductor in the pure limit and for arbitrary finite amounts of impurity scattering has been reported by Jiang and Carbotte [32]. To illustrate their results, they assumed cylindrical symmetry with tight-binding hopping probabilities for motion perpendicular to the plane and free electron propagation in the planes. They

found that the pure and dirty limits are not suitable for the study of anisotropy and that these effects show up most clearly in the conductivity for intermediate impurity scattering. Hirachfeld et.al. [33] calculated the microwave conductivity of a $d_{x^2-y^2}$ superconductor in the presence of a elastic impurity and inelastic scattering due to antiferromagnetic spin fluctuations. The low-temperature conductivity does not simply reflect the linear temperature dependence of the number of quasiparticles in a d-wave system, as often suppressed. Hayward et.al.[34] calculated $\sigma_1(\omega)$ of a doped two leg t-j ladder for an electric field polarized parallel to the legs of the ladder. It is shown that low-and high electron density regimes differently exhibiting Tommanga-Luttinger and Luther-Emery like behaviour, respectively. They concentrated on the hole-doped region where the conductivity has a Drude-weight proportional to the hole-doping and on apparent threshold absorption (a pseudogap) which may be associated with the energy to break a pair. This pseudogap in $\sigma_1(\omega)$ is present even though the pairs have modified $d_{x^2-y^2}$ like wave function because the geometry of the ladder leads to quasiparticle states which probe the gap along an antinode.

Atkinson and Carbotte [35] calculated c -axis optical conductivity, $\text{Re}[\sigma_1(\omega)]$ in the high- T_c superconductors in the superconducting state. The basic premises of this work is that electron tunneling along c -axis between adjacent CuO_2 layers must pass through intervening layers. They have also reported that, for weak interlayer coupling, it is preferable for electrons to travel along the c -axis by making a series of interband transition rather than to stay within a single (and very narrow) band. It was reported further by them that many of the properties of the normal state optical conductivity including the pseudogap can be explain by interband transitions. They found that while the onset of superconductivity is clearly evident in the spectrum, there is no clear signature of the symmetry of the superconducting order parameter. The

reflectivity in the superconducting and normal state of $\text{YBa}_2\text{Cu}_3\text{O}_{7.8}$ has been reproduced with the effective medium theory plus an anisotropic dielectric function and the Mattis-Bardeen conductivity with a gap value $2\Delta/k_B T_c = 2.5$ to 2.7 by Noh et.al. [36]. They found that the lowest IR-active phonon polarized in high conductivity plane produces structure in the superconducting gap. The lowest frequency phonon perpendicular in the plane is overdamped and electronic susceptibility is more anisotropic for $\text{YBa}_2\text{Cu}_3\text{O}_{7.8}$ than for $\text{La}_{1.85}\text{Sr}_{0.15}\text{CuO}_{4.8}$.

Analysis of a - b plane conductivity for both twinned and untwinned $\text{YBa}_2\text{Cu}_3\text{O}_{7.8}$ as a function of temperature and doping shows that below a well defined temperature T^* a dip in the spectrum symmetrically appears separating the infra-red charge excitation spectrum into two components with distinct energy state. The charge from monotonic in σ^{ab} is found to be concurrent with the onset-of-phonon anomalies in Raman and infra-red spectra below T^* . The optical data are suggested to the evidence for the appearance of an inhomogenous distributions of carriers rather than the opening of a simple gap for charge excitation below T^* . An interpretation which is consistent with angle-resolve photoemission and electronic Raman spectra. It has been suggested that the behaviour below T^* and the absence of any anomalies in T can be interpreted assuming a Bose-Einstein condensation of performed pairs [37].

Analysis of optical conductivity measured for cuprates has been done via the dopped Hubbard model in infinite dimensions using the analytical variant of the dynamic Lanczos method. Kee et.al. [38] examined the frequency behavior in the low frequency region at comparatively large doping, the midinfra-red band and isobestic point in the optical conductivity of cuprates. They demonstrated that these features shown in infinite dimensions are the

general features of strong correlation. Polaronic features similar to those observed in the photoinduced spectra of cuprates have also been detected in reflectivity spectra of chemically doped parent compounds of HTSC, both n-type and p-type. In $\text{Nb}_2\text{CuO}_{4-y}$ these features, whose intensities depend both on doping and temperature, include local vibrational modes in the far infra-red and a broad band centred at 1000 cm^{-1} . The lattice band is produced by the overtone of two (or three) local modes and is well described in terms of small-polaron model, with a binding energy of about 500 cm^{-1} . Most of the above infra-red features are shown to survive in the metallic phase of $\text{Nb}_{2-x}\text{Ce}_x\text{CuO}_{4-y}$, $\text{Bi}_2\text{Sr}_2\text{CuO}_4$ and $\text{YBa}_2\text{Cu}_3\text{O}_{7-y}$, where they appear as extra Drude peaks. The occurrence of polarons is attributed to local modes strongly coupled to carriers as shown by a comparison with tunneling results [39].

Tsvetkov et.al [40] reported infra-red reflectivity measurement of the *a-b* plane response of superconducting $\text{Bi}_2\text{Sr}_2\text{CuO}_4$ single crystal. The frequency dependent conductivity has a maximum near 500 cm^{-1} at room temperature, which shifts to lower temperature and merges with a Drude peak below 100 K. They attributed the unusual behavior of the midinfra-red conductivity to low frequency transition between electronic bands of mainly BiO character near the M point. The linear temperature dependent of the low frequency resistivity can be followed down in approximately 40 K where it saturates. The real and imaginary parts of optical conductivity ($\sigma_1+i\sigma_2$) of partly untwinned YBCO thin films were measured by Pimenov et.al. [41], using submillimeter spectroscopy from frequencies 100 GHz to 1 THz. The frequency dependence of the conductivity below T_c can be described by a narrow Drude-like peak with strongly temperature dependent relaxation rates. $\sigma_1(\omega)$ does not extrapolate to the universal d-wave value of 0 K. They presented $\sigma_1(\omega)$ in the spectrum range from 0.1-100 THz.

The use of the two-fluid model for analyzing microwave conductivity of YBCO is critically applied for s-wave and d-wave. The weak and strong scattering in the light of published results on single crystals and of results presented on high quality epitaxial films and powdered doped with Zn and Co [42]. It is argued that the normal electrons in the best sample show non local conductivity ($\lambda < 1$ below 40 K) and this provides a natural explanation of the low temperature behavior of the measured surface impedance, if correct this model firmly in favour of d-wave pairing. Evidence is shown that some 10% of electrons remains normal at $T=0$ in good films and 50% or more in heavily doped powders, in state which may or may not be localized. The behavior is associated with a T^2 -term in the temperature dependence of the λ and is in the accord with recent calculation of the strong scattering impurities. It is argued that in the superconducting state transport between localized state is not necessarily associated with hopping conduction, because of the effective Andreev reflection. Measurements by Waldram et.al. [43] of the surface impedance of good quality optimized YBCO film have given results for the complex conductivity. They concluded that below 40 K, the normal electrons enter the anomalous skin-effect regime. They also mentioned that if their analysis of this situation proves to be correct it would provide some evidence that the velocity of the dominant excitation at least approximately to the band structure.

1.5.2 Behavior of dynamical conductivity and surface resistance with temperature

It has been known for some time that the normal state d. c. conductivity of the cuprates is strongly enhanced well above the thermodynamical transition temperature T_c . Specific heat measurements on highly homogenous single crystal

show evidence of a peak at T_c , where BCS (mean field) theory says that only a discontinuity should appear. Recently experimental evidence obtained from penetration depth measurements also suggests that the 3D x - y optical fluctuation exit down to 9 K below T_c . Analge et. al. [44] studied on fluctuation in the microwave conductivity of cuprates in normal state. Microwave surface impedance measurements on a high quality single crystal of YBCO shows a linear in T increase of the penetration depth at low temperature [45]. The twinned YBCO crystal typically show zero dc resistance at 92-93 K with a normal state resistivity at 100 K [46]. The enhanced conductivity above T_c has been measured by many groups at dc [46,47], they manifested the data by a conductivity which diverges more quickly than the theoretical predictions.

Recent measurements of microwave THz and infra-red frequencies have revealed a peak in σ_1 below T_c . Based on THz measurements, which were performed on high quality single crystal films of YBCO (900 Å⁰ and 500 Å⁰), it has been found that σ_1 features a peak which increases with amplitude and shifts to lower temperature as frequency changes from 1.2 to 0.4 THz. Although the quasiparticle relaxation time extracted from these results using the two-fluid model exhibits an enhancement below T_c . The analysis may not adequate to account for frequency dependent σ_1 by fitting the Mattis-Bardeen theory (modify to include scattering) using a slower average rate of increase of the anisotropic gap than for the BCS case as temperature decreases below T_c . This is consistent with the higher normal fluid density (higher than Gorter-Casimir value) from the two-fluid model interpretation of THz results. It has be taken as an evidence of BCS coherence factor in a high- T_c superconductor with a slower gap than BCS gap increases below T_c . Frankel et.al [48] discussed the role of coherence factor to account for the presence of the conductivity peak and the absence of the peak in NMR relaxation rate. Furthermore, they presented a

model for the quasiparticle relaxation time measured by Femtosecond pump probe spectroscopy. This model allows a fit to the temperature dependent energy gap function which is also consistent with the slower gap increase below T_c .

Broun et.al [49] calculated in-plane microwave conductivity of nearly optimally doped single crystal of $Tl_2Ba_2CuO_{6+\delta}$ (Tl-2201) at 14.4, 34.8 and 35.9 GHz with $T_c=98$ K using cavity perturbation methods. At low temperature the in-plane penetration depth has a strong linear temperature dependence, indicative of an unconventional pairing state with line nodes. The real part of conductivity shows a broad frequency-dependent peak near 30 K, similar to that seen in $YBa_2Cu_3O_{7-\delta}$ and $Bi_2Sr_2Cu_2O_8$ crystals. With tetragonal crystal symmetry and a single CuO_2 plane per unit cell. Tl-2201 is the simplest structure so far to display these features. Surface resistance data also contribute significantly to current understanding of the cuprates. Measurements made on high quality YBCO crystal by Bonn et al [50] show that R_s falls simply by several orders of magnitude on cooling through T_c . The value of $\sigma_1(T)$ deduced from the data display, a broad peak near about 45 K and a two-fluid interpretation shows that τ rises rapidly on entering the superconducting state, suggesting that inelastic scattering in the normal state is primarily of electronic origin, before saturating at intermediate temperature. Measurements on BSCCO [51] also reveal a broad peak in $\sigma_1(T)$ but do not exhibit nonmonotonic $R_s(T)$ as of YBCO.

Jiang et. al. [52] measured surface impedance and surface inductance for films prepared by the laser ablation technique. They observed that surface resistance at 21 GHz decreased by about three orders of magnitude as the temperature decreased from 90 K to 80 K reaching a low value of $4.9 \times 10^{-4} \Omega$. Measured London penetration depth, λ and coherence length, ξ were found anisotropic. Their value depends on the direction of the microwave electric field

relative to the c -axis. They deduced the value of $\lambda_{||}(0)$ to be about 1800 Å, $\lambda_{||}(86.5)$ about 8000 Å and $\lambda_{\perp}(86.5)$ about 26000 Å, where $\lambda_{||}(0)$ is the penetration depth (as $T \rightarrow 0$ K) for the electromagnetic electric field parallel and λ_{\perp} perpendicular to the film plane. In addition $\xi_{||}$ was determined to be 129 Å, ξ_{\perp} to be equal to 40 Å at 86.5 K. The anisotropic factor γ is about 3. The electromagnetic surface impedance of layered superconductors has been estimated within the frame-work of BCS theory. The dependence on the coherence length and the mean free path of the electrons, the ambient temperature and the frequency of the incident microwave have been calculated by Chang et al [53] for a c -axis normal oriented film.

Epitaxial thin film of $\text{YBa}_2\text{Cu}_3\text{O}_{7.8}$ with low cation and oxygen disorder exhibits two features in the temperature dependence of the microwave surface impedance which are consistent with a weak s -wave superconducting state associated with the CuO chains [54]. First both the microwave surface resistance and magnetic field penetration depth exhibits a weak exponential temperature dependence below 30 K, corresponding to an energy gap of about 6 meV. Second the penetration depth exhibits a small hump at about 60 K, which is consistent with a two band BCS calculation using 6 meV for the smaller gap.

Observation on the surface impedance at 14, 25 and 36 GHz of high quality crystals of $\text{Bi}_2\text{Sr}_2\text{CaCu}_2\text{O}_{8+x}$ (Bi-2212), $\text{Tl}_2\text{Ba}_2\text{CuO}_6$ (Tl-2201) and $\text{YBa}_2(\text{Cu}_{0.975}\text{-Zn}_{0.025})_3\text{O}_{7.8}$ (Y123/Zn) are reported and the corresponding complex conductivity $\sigma = \sigma_1 - i\sigma_2$ is analyzed in the critical region near T_c and at higher temperature where fluctuations are important [43]. The well known sharp peak in σ_1 within the critical region is successfully analyzed using effective medium theory. At higher temperatures Bi-2212 and Y123/Zn agree in form with the treatment of conductivity fluctuations of Asdamazov and Larkin,

extended to high frequency Tl-2201, however, shows an extra response of long relaxation time which persists at high temperature. Tentative explanations of this effect are considered, including the possibility that it is due to uncondensed bipolarons. The physics of conversion at super current to normal current within fluctuating regions is reviewed.

1.5.3 Penetration depth and Relaxation time

Optical conductivity measurements shows that high temperature superconductor exhibits a number of anomalies when compare with the usual Drude like Fermi-liquid behavior found in conventional metals. Experimental measurements shows that effective transport scattering rate $1/\tau(\omega)$ exhibits linear-in- ω behavior over a wide frequency range, while the measurement of Puchkov et.al.[55] demonstrate the significant deviation from this standard behavior occurred especially in underdoped material at low temperature in the so called pseudogap regime, where $1/\tau(\omega)$ is strongly suppressed [56]. Microwave measurements have been important in establishing the nature of cuprate electrodynamics with penetration depth data from high quality YBCO crystal [57]. In YBCO, a linear temperature dependence of penetration depth at low temperatures was observed and indicated the presence of low-lying excitation. Using untwinned crystal, this behavior later shown to occur separately for current flowing in the a and b direction [58] suggesting that the unconventional response was not due solely to the Cu-O chain layers. Recent measurements [51,59] on BSCCO single crystal also show that $\Delta\lambda \propto T$ at low T and support this view as in YBCO. BSCCO has CuO₂ bilayer, but Cu-O chain layer are absent. It seems likely that structural vibrations between the different compounds are affecting the superconductivity.

The temperature dependence of the penetration depth of superconductor normal metal-multilayered metals has been calculated from Eliashberg theory. The results reported have been focused on YBCO but the conclusion apply to any system of proximity coupled bilayer [60]. Calculations show that depleting the chains of oxygen and consequently the appearance of gaplessness leads to a transition from an experimental dependence to a power law, initially linear then quadratic. Different analytical dependences have been measured by various groups, and conflicting conclusions have been made about the pairing state in the cuprate superconductors. Non-linear conductivity, skin effect and transport across a barrier are proposed as experiments for a direct study of in-plane anisotropy of the electron life time in the cuprates. The magnitude of these effects within the proposed cold-spot model of the normal state of the cuprates is estimated. A modification of the cold-spot model yielding magneto transport in agreement with experiments is proposed [61]. Kresin and Wolf calculated the electro-magnetic penetration depth for the normal metal side of a proximity junction including paramagnetic impurities in the strong scattering model [62]. Pair breaking strongly affects the results and low temperature behavior is sensitive to the location of the states in the gap. They have also computed the frequency dependence of the optical conductivity and find structure in the gap on the normal metal side which similar to that found in the intrinsic case. Atkinson et.al. [63] calculated the penetration depth in a , b and c direction for a simple model of YBCO. In this model, they considered two layers -representing CuO_2 planes and Cu-O chain per unit cell. Further, BCS type pairing for both s-wave and d-wave were considered. The Cu-O chain become superconducting at temperature lower than T_c , because of their proximity to the planes and there is no induced gap in the b -direction (along the chain) is sensitive to the size of the induced gap, the difference between the shapes of the penetration depth curves in the a and b direction reveals a great deal about the nature of the condensate in the chain. They found that in their proximity model there are always regions of

chain Fermi-surface on which the induced gap is much smaller than T_c , so that the temperature dependence of λ_b is always different than that of λ_a . Experimental observation of a - b anisotropy shows nearly identical temperature dependence.

Measurements on microwave surface impedance $Z_s = R_s + iX_s$ have play a key role in further understanding of high- T_c superconductors. A term, linear at low T , in the temperature dependent in-plane penetration depth, $\lambda^{ab}(T)$ first observed in single crystal of YBCO by Hardy et.al. [57]. The non monotonic T -dependence of a - b plane surface resistance R_s^{ab} observed by Bonn et.al. [64-65] has been interpreted in terms of effective quasiparticle scattering rate- τ that increases rapidly below T_c before saturating at what is suggested to be an elastic impurity scattering limit. This qualitative picture is inconsistent with dominant electron-electron scattering above T_c , which is rapidly suppressed below T_c , as the charge carriers condensed into superfluid. Doping in small amount causes decrease in R_s^{ab} as increasing scattering. Wu et.al. [66] found that both R_s^{ab} and λ_s^{ab} are in accord with BCS theory. Ma et.al. [67] have suggested that the Cu-O chain layer may play a significant role in the unconventional microwave response of YBCO. However, a - b plane anisotropy measurements [33] on untwinned YBCO single crystal suggested that the Cu-O chain layers affects only the magnitude of R_s^{ab} and λ_s^{ab} rather than their forms as a function of T .

1.5.4 Collective excitation modes

The collective excitation in layered narrow tight-binding band superconductors, were investigated within the ladder diagram approximation with vacuume-polariozation correction [68]. The in-plane nearest-neighbor interaction and the interplane nearest-neighbor tunneling are assumed. For the

extended s-wave and d-wave states, the in-plane and out-of plane longitudinal plasma frequencies (plasma energies) in the long wave length limit were calculated as a function of hole density and temperature T . Their expression almost coincide with those for the normal state electrons in the same tight-binding model. Both of the in-plane and out-of plane results are almost unaffected by the anisotropy of the order parameter and almost do not depends on T . The out-of plane plasma frequencies can be smaller than superconducting gap for the extended s-wave state. The obtained in-plane and out-of plane plasma frequencies (though they are for longitudinal modes) show good agreement with experimental results for the transverse plasma frequency in high- T_c superconductors. Belitz et.al. [69] used the exact eigen state formalism to construct a gauge variant theory for correlation function for disordered superconductors. The density response and the longitudinal and transverse current response at zero temperature were calculated explicitly for BCS superconductors with arbitrary amount of disorder. At small frequencies and wave numbers they discussed the coherence length, the penetration depth and the Anderson- Bogoluibov modes at various degrees of disorder. It has been found that the disorder does not change the absence of low-lying collective modes in charge superconductors. Implication for the quasiparticle inelastic lifetime were also discussed.

Fertig and Das Sarma [70] investigated the collective mode spectrum for a layered superconductor structure. For wave vector directed close to the superlattice axis, they found that the plasmon modes remains below the superconducting gap edge. This is in sharp contrast with the situation for isotropic superconductors in three dimension, for which Anderson-Higgs mechanism lifts all such modes out of the gap. They also found that as a mode crosses the gap edge, either by increases the wave vector or tilting its direction with respect to the superlattice axis, there is a unique mode coupling effect

between pair breaking excitations and the collective modes. This manifest itself as a line splitting in the dielectric regions, which may in principle, be used to determine the gap of such a system. They also calculated the effect of interplane tunneling on the collective mode spectrum. It was found that if the tunneling rate is large enough, the plasma mode may all be lifted out of the gap. It was mentioned that estimates for the plasmon energy based on the effective mass approximation can grossly overestimates its minimum value. The model of a layered structure constituted by two periodical arranged London superconducting layers is considered in the linear steady-current regime by Ivanchenko [71]. The model admits exact solutions in a quite general situation. The use of these solutions allows one to derive differential equations describing the steady-current electrodynamics in the limit, when characteristic penetration length essentially exceed the period of the structure. The intuitive idea that the structure in this limit can be described as an anisotropic medium is only partially confirmed. The London equation has appropriate anisotropic form, but Maxwell'equation bear additional features. A magnetic field divided in to components: normal to layers and two parallel, longitudinal and transverse, is not affected as it should be a uniaxial medium. The normal and longitudinal components are not influenced essentially by the structure, while the transverse component is essentially screened. It has been argued that this screening effect is a common feature of layered structure not related to the model.

The plasma oscillations in a superconductor are investigated for the case when plasma energy is smaller than the superconducting gap. Ohasi and Takada [72] proposed that the plasma energy has a temperature dependence in dirty superconductors when the strength of the impurity scattering exceeds a critical value, the plasma disappears at the transition temperature T_c as observed in high- T_c cuprates, $(\text{Bi}_2\text{Sr}_2\text{CaCu}_2\text{O}_{8+\delta})$. They also study the coupling of the plasma with Carlson-Goldman (CG) mode in dirty superconductors. A pole analysis

show that the coupling occur just below T_c . However even in this situation, it was found that two different mode like peak structure can be still observed in spectra of the density-density correlation function and the structure function of the pair field susceptibility.

1.6 Scope of thesis

There have been several experimental as well as theoretical studies on dynamical conductivity in normal state and superconducting state of cuprate superconductors. Some of the theoretical studies are quite elaborated and rigorous. However their comparison with experimental data is poor and they lack the simplicity needed to make the qualitative understanding of basic physics of the cuprate superconductors. Aim of this thesis has been to perform a simple model calculation of dynamical conductivity and collective excitations in cuprate superconductors, in order to understand the basic physics (derived from experimental measurements) in a simple manner. To perform our calculation, we modeled cuprate superconductors as layered structures of Cu-O conducting layers embedded into a dielectric medium, where a weak coupling between Cu-O conducting layers is allowed. Our calculations of dynamical conductivity and collective excitations in normal state are presented in chapter-II. In chapter-III, we present our calculations on dynamical conductivity, surface resistance, relaxation time and collective excitations in superconducting state. Summary of chapter I to III is given in chapter-IV.

REFERENCES

- [1]. Charles P. Poole Jr., Horacio A., Farach Richard, J. Creswick,
“*Superconductivity*”, Pul. Academic Press, USA (1995), pp-188.
- [2]. Cava R. J., Batlogg B., Chen C. H., Rietman E. A., Zahurak S. M., Werder D.,
Nature **329** (1987), 423.
- [3]. Monod P., Ribault M., D’Yvoire F., Jegoudez J., Colline G.,
Revoleschi A., *J. Phys.* **48** (1987), 1369.
- [4]. Tokumoto M., Ihara H., Matsubara T., Hirabayashi M., Terada N., Oyanagi H.,
Murata K., Kimura Y., *Jpn. J. Appl. Phys.* **26** (1987), L1566.
- [5]. Ravean B., Deslanddas F., Michel C., Hervien M., Proc. *Intern. Meeting
on High- T_c Superconductors*, Schloss Mauterndorf, Feb. 1988, “*High- T_c
Superconductors*”, Ed. Weber H. W., Plenum N.Y.-3 (1988).
- [6]. Charles P. Poole Jr., Horacio A., Farach Richard, J. Creswick,
“*Superconductivity*”, Pul. Academic Press, USA (1995), pp-194.
- [7]. Charles P. Poole Jr., Horacio A., Farach Richard, J. Creswick,
“*Superconductivity*”, Pul. Academic Press, USA (1995), pp-194.
- [8]. Charles P. Poole Jr., Horacio A., Farach Richard, J. Creswick,
“*Superconductivity*”, Pul. Academic Press, USA (1995), pp-195.
- [9]. Charles P. Poole Jr., Horacio A., Farach Richard, J. Creswick,
“*Superconductivity*”, Pul. Academic Press, USA (1995), pp-197.
- [10]. Charles P. Poole Jr., Horacio A., Farach Richard, J. Creswick,
“*Superconductivity*”, Pul. Academic Press, USA (1995), pp-197.
- [11]. Charles P. Poole Jr., Horacio A., Farach Richard, J. Creswick,
“*Superconductivity*”, Pul. Academic Press, USA (1995), pp-197.
- [12]. Charles P. Poole Jr., Horacio A., Farach Richard, J. Creswick,
“*Superconductivity*”, Pul. Academic Press, USA (1995), pp-198.
- [13]. Charles P. Poole Jr., Horacio A., Farach Richard, J. Creswick,
“*Superconductivity*”, Pul. Academic Press, USA (1995), pp-200.

- [14] K. Kitazawa , H. Takagi, K. Kishio, T. Hasagawa , S. Uchida , S. Tagima
S. Tanaka, K. Fueki, **Physica C 153** (1988), 9.
- [15] K. Kitazawa, **IMB J. Res. Dev.** **33** (1989), 201.
- [16] J. G. Bednorz, M. Takashige , K. A.Muller, **Europhys. Lett.** **3** (1987), 379.
- [17] S. Uchida, H. Takagi, K. Kitazawa, S. Tanaka, **Jpn. J. Appl. Phys.** **26**
(1987), L1.
- [18] Y. Iye, In “*Mechanisms of High Temperature Superconductivity*”, Ed.
by H. Kamimura, A. Oshiyama, **Springer Ser. Mater. Sci.** **11** (1989), 263.
- [19] S. Kambe, K. Kitazawa, M. Naito, A. Fukuoka, I. Tanaka, H. Kojima,
Physica C160 (1989), 35.
- [20] K. K. Singh, P. Ganguly, J. B. Goodenough, **J. Solid State Chem.** **52**
(1984), 254.
- [21] Charles P. Poole Jr., Horacio A., Farach Richard, J. Creswick,
“*Superconductivity*”, Pul. Academic Press, USA (1995), pp-226.
- [22] Charles P. Poole Jr., Horacio A., Farach Richard, J. Creswick,
“*Superconductivity*”, Pul. Academic Press, USA (1995), pp-227.
- [23] Charles P. Poole Jr., Horacio A., Farach Richard, J. Creswick,
“*Superconductivity*”, Pul. Academic Press, USA (1995), pp-227.
- [24] J. Annett, N. Goldenfeld and A. J. Leggett, In *Physical Properties of High
Temperature Superconductors-V*, Ed. by D. M. Ginsberg (World
Scientific, Singapore 1996).
- [25] J. R. Waldram et. al., **Phys. Rev.** **B55** (1997), 3222 and A. J. Berlinsky et. al.
Phys. Rev. **B48** (1993), 4074.
- [26] S. B. Nam, **Phys. Rev.** **156** (1967), 470.
- [27] G. Brandi and A. J. Sievers, **Phys. Rev.** **5** (1972), 3350.
- [28] N. E. Bickers, D. J. Scalapino, R. T. Collins and Z. Schlesinger,
Phys. Rev. **B42** (1990), 67.
- [29] D. B. Tanner et. al., **J. Phys. Chem. Solids** **53** (1992), 1611.

- [30] T. Timusk and D. B. Tanner, in “*Physical Properties of High Temperature Superconductors*”, Ed. by D. M. Ginsberg (World Scientific, Singapore), Vol. I (1989), 339 and Vol. III (1992), 363.
- [31] K. Kamaras et al., *Phys. Rev. Lett.* **59** (1987), 919.
- [32] C. Jiang, J. P. Carbotte, *Phys. Rev.* **B53** (1996), 12400.
- [33] P. J. Hiraschfeld, W. O. Putikka, D. J. Scalapino, *Phys. Rev. Lett.* **71** (1993), 3705.
- [34] C. A. Hayward, D. Poilblanc and D. J. Scalapino, *Phys. Rev.* **B53** (1996), R8863.
- [35] W. A. Atkinson and J. P. Carbotte, *Phys. Rev.* **B55** (1997), 12748.
- [36] T. W. Noh, P. E. Sulewski and A. J. Sievers, *Phys. Rev.* **B36** (1987), 8866.
- [37] D. Mihailovic, T. Mertelg and K. A. Muller, *Phys. Rev.* **B57** (1998), 6116.
- [38] Hae-Young Kee and Jongbae Hong, *Phys. Rev.* **B55** (1997), 5670.
- [39] P. Calvani, M. Capizzi, S. Lupi, P. Maselli, A. Paolone and P. Roy, *Phys. Rev.* **B53** (1996), 2756.
- [40] A. A. Tsvetkov, J. Schutzmann, J. I. Gorina, G. A. Kaljushnaia and D. van der Marel, *Phys. Rev.* **B55** (1997), 14152.
- [41] A. Pimenov, A. Loidl, G. Jakob and H. Adrian, *Phys. Rev.* **B59** (1999), 4390.
- [42] J. R. Waldram, P. Theopistou, A. Porch and H. M. Cheah, *Phys. Rev.* **B55** (1997), 3222.
- [43] J. R. Waldram, D. M. Broun, D. C. Morgan, R. J. Ormeno and A. Porch, *Phys. Rev.* **B59** (1999), 1528. and references therein.
- [44] S. M. Analge, J. Mao, J. C. Booth, Dong Ho Wu. and J. L. Peng, *Phys. Rev.* **B53** (1996), 2792.
- [45] J. Mao et al., *Phys. Rev.* **B51** (1995), 3316.
- [46] T. A. Freedmann et al., *Phys. Rev.* **B39** (1989), 4258.
- [47] S. J. Hagen, Z. Z. Wang and N. P. Ong, *Phys. Rev.* **B38** (1988), 7137.

- [48] A. Frenkel, F. Gao, Y. Liu, J. F. Whitaker, C. Uher, S. Y. Hou and J. M. Phillips, **Phys. Rev. B54** (1996), 1355.
- [49] D. M. Broun, D. C. Morgan, R. J. Ormeno, S. F. Lee, A. W. Tyler, A. P. Mackenzie and J. R. Waldram, **Phys. Rev. B56** (1997), R11443.
- [50] D. A. Bonn et. al., **Phys. Rev. Lett. 68** (1992), 2390.
- [51] S. F. Lee et. al., **Phys. Rev. Lett. 77** (1996), 735.
- [52] H. Jiang, T. Yuan, H. How, A. Widom, C. Vittoria, D. Chrisey, J. Horwitz and A. Drehman, **Phys. Rev. B49** (1994), 9924.
- [53] J. J. Chang and D. J. Scalapino, **Phys. Rev. B40** (1989), 4299.
- [54] N. Klein, N. Tellmann, H. Schulz, K. Urban, S. A. Wolf and V. Z. Kresin, **Phys. Rev. Lett. 71** (1993), 3355.
- [55] A. V. Puchkov, D. N. Basov and T. Timusk, **J. Phys. (Condens. Mat.) 8** (1996), 10049.
- [56] B. P. Stojkovic and D. Pines, **Phys. Rev. B56** (1997), 11931.
- [57] W. N. Hardy et. al., **Phys. Rev. Lett. 70** (1993), 3999.
- [58] K. Zhang et. al. **Phys. Rev. Lett. 73** (1994), 2484.
- [59] T. Jacobs et. al., **Phys. Rev. Lett. 75** (1995), 4516.
- [60] S. D. Adrian, M. E. Reeves, S. A. Wolf and V. Z. Kresin, **Phys. Rev. B51** (1995), 6800.
- [61] R. Hlubina, **Phys. Rev. B58** (1998), 8240.
- [62] V.Z.Kresin and S.A.Wolf, **Phys. Rev. B46** (1992),6458 ;
Physica C 198(1992),328.
- [63] W. A. Atkinson and J. P. Carbotte, **Phys. Rev. B52** (1995), 10601.
- [64] D. A. Bonn, P. Dosanjh, R. Liang and W. N. Hardy, **Phys. Rev. Lett. 68** (1992), 250.
- [65] D. A. Bonn et. al., **Phys. Rev. B50** (1994), 4051.
- [66] D. H. Wu et.al., **Phys. Rev. Lett. 70** (1993), 85.
- [67] Zhengxiang Ma et. al., **Phys. Rev. Lett. 71** (1993), 781.
- [68] S. Missawa, **Phys. Rev. B53** (1996), 2241.

- [69] D. Belitz, S. De Souza-Machado, T. P. Devereaux and D. W. Hoard, **Phys. Rev. B** **39** (1989), 2072.
- [70] H. A. Fertig and S. D. Sarma, **Phys. Rev. B** **44** (1991), 4480.
- [71] Yu. M. Ivanchenko, **Phys. Rev. B** **48** (1993), 15966.
- [72] Y. Ohashi and S. Takada, **Phys. Rev. B** **59** (1999), 4404.